

Biophysical Journal, Volume 112

Supplemental Information

**Mechanosensitive Adhesion Explains Stepping Motility in Amoeboid
Cells**

**Calina A. Copos, Sam Walcott, Juan C. del Álamo, Effie Bastounis, Alex
Mogilner, and Robert D. Guy**

Mechanosensitive adhesion explains stepping motility in amoeboid cells

C. A. Copos, S. Walcott, J. C. del Álamo, E. Bastounis, A. Mogilner, R. D. Guy

Supplementary Material

S.1 Experimental materials and methods

The experimental protocols used to culture *Dictyostelium* cells and quantify the mechanics of their chemotactic migration were described at length in our previous studies [1–5]. The key steps of these protocols are summarized below.

Cell culture and microscopy. *Dictyostelium discoideum* cells were grown under axenic conditions in HL5 growth medium in tissue culture plates. This study reports on six different cell lines: wild type Ax2 and Ax3, myosin II null, myosin II essential light chain null, scrA null, and talin A-null cells. All the cell lines were obtained from the Dicty Stock Center, except for the talin null cells which were a gift from M. A. Titus (University of Minnesota, Minneapolis, MN). Aggregation competent cells were prepared by pulsing 5×10^6 cells/ml suspension in Na/K phosphate buffer (9.6 mM KH₂PO₄, 2.4 mM Na₂HPO₄, pH 6.3) with cAMP to a concentration of 30 nM every 6 minutes for 6 hours. Cells were seeded onto the functionalized polyacrylamide substrate and allowed to adhere. A drawn glass capillary mounted on a micromanipulator served as the source of chemoattractant (150 mM cAMP in an Eppendorf femtotip, Eppendorf, Germany). To identify the cell contours, differential interference contrast (DIC) images were acquired using a 40X air objective. A custom algorithm using MATLAB (Mathworks Inc., Natick, MA) identified the contour of the cells [6].

Polyacrylamide gel preparation. We fabricated 12-mm diameter, ~ 40 μ m-thick polyacrylamide gels of 4% acrylamide and 0.056% bisacrylamide (~ 900 Pa [7]) on 22-mm square #1 glass coverslips [8, 9]. We mounted the coverslips with the gels in Petri dishes with a circular opening in the bottom using silicon grease (Dow Corning, Midland, MI). Our gels consist of two layers: the bottom layer contains no beads, and the upper one contains 0.04% carboxylate modified red latex beads of 0.1 μ m diameter (FluoSpheres; Molecular Probes, Eugene, OR). We made the gels physiologically compatible by crosslinking collagen I to the surface of the polyacrylamide. We used 1 mM Sulfo-SANPAH (Thermo Sci., Rockford, IL) after UV activation to crosslink 0.25 mg/ml collagen I. To test the effect of increased substratum adherence, 20 mg/ml of poly-L-Lys (MW=30000-70000, P9155 Sigma-Aldrich) were mixed together with the collagen solution, while the remaining protocol steps were the same as described above. Different concentrations of poly-L-lysine were tested, and the one selected was chosen since wild-type cells were still able to chemotax, but with deeply decreased speed. The gels were incubated overnight at room temperature. After washing, the gels were stored in Na/K phosphate buffer (9.6 mM KH₂PO₄, 2.4 mM Na₂HPO₄, pH 6.3, same composition as used in the experiments) and antibiotic (40 μ M Ampicillin) for up to a week.

Three-dimensional force microscopy (3DFM). We imaged z-stacks containing fluorescent beads, consisting of 24 planes separated 0.4 μ m from each other and acquired images every 5 seconds. The 3D substrate deformation was determined for each z-stack via image cross-correlation with a non-deformed reference z-stack,

which was obtained after the cell moved out of the field of view. Both instantaneous and reference z-stacks were divided into 3D interrogation boxes of size $24 \times 24 \times 24$ pixels to balance resolution and signal-to-noise while minimizing phototoxic effects. These settings provided a Nyquist spatial resolution of $2.1 \mu\text{m}$. Using the measured deformations as boundary conditions, we computed the three-dimensional stresses generated by the cells on the substrate using the 3D Green's function of the elastic equation given by del Álamo et al. [10].

S.2 The full model equations

In our two-dimensional model the cell is crawling in the horizontal direction with surface attachments between the cell and the surface below it. The cell membrane and its underlying cortex are represented as one structure with position $\mathbf{X}(s, t) = (x(s, t), y(s, t))$ where t is time and s is a local parametric coordinate on the structure. Here, \hat{x} is a unit vector in the horizontal direction of crawling while \hat{y} is in the vertical direction. The system is described by the following force-balance equation:

$$\xi \frac{\partial \mathbf{X}}{\partial t} = \mathbf{F}_{\text{membrane/cortex}} + \mathbf{F}_{\text{pressure}} + \mathbf{F}_{\text{polymerization}} + \mathbf{F}_{\text{cytoskeleton}} + \mathbf{F}_{\text{surface}}. \quad (\text{S1})$$

The cell experiences a velocity-dependent drag with the environment where ξ denotes the viscous drag coefficient. Below, we present the constitutive laws for the forces in the force-balance equation.

- The elastic response of the membrane/cortex structure:

$$\mathbf{F}_{\text{membrane/cortex}} = \frac{\partial}{\partial s} \left[\left(\gamma + k(|\partial \mathbf{X} / \partial s| - 1) \right) \hat{\tau} \right] \quad (\text{S2})$$

where γ is the resting tension and k is the stiffness of the material. The tangent vector to the curve $\mathbf{X}(s, t)$ is defined as $\hat{\tau} = \partial_s \mathbf{X} / |\partial_s \mathbf{X}|$ where $\partial_s \mathbf{X} = \partial \mathbf{X} / \partial s$.

- The cytosol is modeled as a viscous medium and is assumed to have a resting internal pressure p_0 and resting volume V_0 . The intracellular pressure force is given by,

$$\mathbf{F}_{\text{pressure}} = \left(p_0 + \kappa_{\text{cell}} \ln(V/V_0) \right) \hat{n}. \quad (\text{S3})$$

Here, κ_{cell} represents the bulk modulus and the normal vector to the curve $\mathbf{X}(s, t)$ is given by $\hat{n} = \partial_s \hat{\tau} / |\partial_s \hat{\tau}|$ where $\hat{\tau}$ is the tangent vector defined above. A flow is volume preserving if $\iint_{\Omega} \nabla \cdot \mathbf{u} dA = \int_{\partial \Omega} \mathbf{u} \cdot \hat{n} ds = 0$ where Ω denotes the interior domain, while $\partial \Omega$ is its boundary. The membrane velocity is given by Eq. S1 and so this condition is met by requiring $\int \mathbf{F} \cdot \hat{n} ds = \xi \int \mathbf{u} \cdot \hat{n} ds = 0$, where \mathbf{F} denotes the sum of the forces from Eq. S1. Thus, the resting pressure is computed by,

$$\begin{aligned} \int \left(\mathbf{F}_{\text{pressure}} + \mathbf{F}_{\text{remaining}} \right) \cdot \hat{n} ds &= 0 \\ \int \left(p_0 \hat{n} + \mathbf{F}_{\text{remaining}} \right) \cdot \hat{n} ds &= 0 \\ p_0 \int ds + \int \mathbf{F}_{\text{remaining}} \cdot \hat{n} ds &= 0 \\ p_0 &= - \frac{\int \mathbf{F}_{\text{remaining}} \cdot \hat{n} ds}{\int ds}. \end{aligned}$$

Here, $\mathbf{F}_{\text{remaining}}$ represents all of the other forces involved in the force balance in Eq. S1. If the equation was solved analytically, this pressure force due to the resting internal pressure would be sufficient to enforce volume conservation. Due to numerical time integration errors, an additional volumetric correction term is introduced to further ensure volume conservation is maintained throughout the simulation.

- The force-velocity relationship for the branching of actin filaments at the leading edge is described by relations of the form, $v = v(F_L)$, where F_L is the force against the protrusion. We assume the following one-dimensional model for the leading edge velocity due to polymerization against the cell membrane,

$$v = \rho_1 e^{-\rho_2 F_L} - \rho_3 . \quad (\text{S4})$$

Force-velocity relations of this form were observed theoretically [16] and experimentally in a certain region of the load forces [17–19]. The constants $\rho_{1,2,3}$ can be determined experimentally through measurements of the force-velocity relationship in directional polymerization of F-actin filaments. An equivalent way to formulate this relation is to assume the polymerization force is a function of the protrusion rate: $F_{\text{polymerization}} = F_{\text{polymerization}}(v)$. Then, the force-balance equation in the direction of motion (Eq. S1) at the cell front has the form:

$$F_{\text{polymerization}}(v) + F_L = \xi v . \quad (\text{S5})$$

To implement the one-dimensional polymerization model in Eq. S5, the force acting against the protrusion, F_L , is computed as a spatial average of the forces acting on the membrane-cortex structure in the region of polymerization. At the cell front, there is no interaction between the membrane-cortex structure and the substrate, and therefore $F_{\text{surface}} = \mathbf{0}$ and $F_{\text{cytoskeleton}} = \mathbf{0}$. Thus, the force against the protrusion is given by the average of the remaining forces at the cell front,

$$F_L = \frac{\int_{\mathcal{P}} |\mathbf{F}_{\text{membrane/cortex}} + \mathbf{F}_{\text{pressure}}| ds}{\int_{\mathcal{P}} ds} . \quad (\text{S6})$$

Given this expression for the ‘load’ force and the polymerization model described in Eqs. S4 and S5, we can solve for an effective driving force, $F_{\text{polymerization}}$, at the leading edge only in the direction of motion. Note that this choice of $F_{\text{polymerization}}$ ensures that the cell front moves with the velocity given in Eq. S4 in the horizontal direction. Using our simulation parameters provided in Table S.1, the effective force-velocity relation at the cell front is shown in Fig. S1.

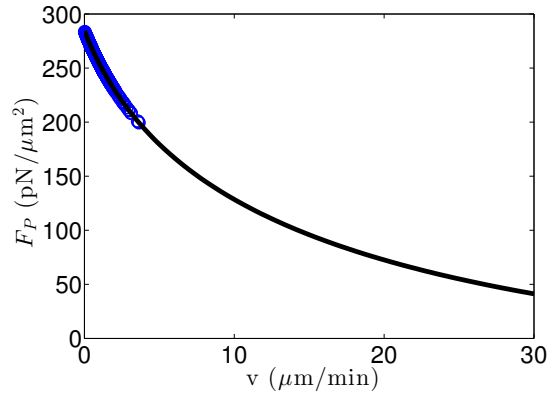


Figure S1: The effective polymerization force-velocity relation at the leading edge. The circles represent the region of velocities and forces in which the simulated cell operates based on the parameters presented in Table S.1 (and also the same parameters used to generate the results in Fig. 6). As the load force increases, the cell front velocity will decrease eventually to zero when the leading edge stalls at a force density of 283 pN/ μm^2 . Stall force of this order of magnitude was experimentally measured [16, 18] and it corresponds to a stall force per filament in the range of $\sim 1\text{-}10$ pN predicted and observed in multiple studies.

- The action of cytoskeleton is to transmit the leading edge polymerization forces to the underlying surface. The protrusive forces at the leading edge are integrated over the region of polymerization and distributed uniformly to the region of cell-surface contact to ensure zero sum of polymerization and cytoskeletal forces,

$$\mathbf{F}_{\text{cytoskeleton}} = -\frac{\int_{\mathcal{P}} |\mathbf{F}_{\text{polymerization}}| ds}{\int_{\mathcal{C}} ds} \hat{x}. \quad (\text{S7})$$

The membrane-cortex structure is within the region of contact, \mathcal{C} , if it is within $5 \mu\text{m}$ of the surface in the vertical direction.

- We assume the cell crawls on top of a flat surface at along the horizontal axis ($y = 0$). The interaction between the cell and the underlying surface is given through both physical adhesive connections and a repulsive force due to contact with the surface:

$$\mathbf{F}_{\text{surface}} = \mathbf{F}_{\text{steric}} + \mathbf{F}_{\text{adhesion}}. \quad (\text{S8})$$

- Below a certain distance, δ_w , the cell feels a nonspecific steric force of the form:

$$\mathbf{F}_{\text{steric}} = -k_{\text{steric}} \left(|y(s, t)| - \delta_w \right) \hat{y} \quad (\text{S9})$$

and is zero otherwise. Here, k_{steric} represents the stiffness of this steric interaction.

- The adhesive force is

$$\mathbf{F}_{\text{adhesion}} = \begin{cases} \zeta N(t, s) (|\mathbf{X} - \mathbf{X}_{\text{surface}}| / \ell_0 - 1) \frac{\mathbf{X} - \mathbf{X}_{\text{surface}}}{|\mathbf{X} - \mathbf{X}_{\text{surface}}|} & \text{if } \frac{|\mathbf{F}_{\text{adhesion}}|}{N} < F_{\text{critical}} \\ 0 & \text{otherwise.} \end{cases} \quad (\text{S10})$$

At each binding site, the adhesive force is the result of the local bond density per adhesion site, $N(t, s)$, a constant adhesive stiffness, ζ , and the elastic deformation of the bond from its resting length, ℓ_0 . Locations of binding along the surface are denoted by $\mathbf{X}_{\text{surface}}$. The position of $\mathbf{X}_{\text{surface}}$ is determined per bond during bond formation; when an adhesive bond forms it binds to the surface directly below the membrane-cortex structure. For the lifetime of the bond, the binding position remains fixed along the surface. The local bond density can vary between zero to full occupancy, $0 \leq N(t, s) \leq 1$.

For the adhesive force, three models are considered for local bond density per adhesion site, $N(t, s)$:

- (1) Uniform slip bonds: $N(t, s) = N = 1$ throughout time and over the entire region of cell-surface contact;
- (2) Non-uniform slip bonds: $N(t, s) = N$ throughout time with

$$N = \begin{cases} 1 & \text{in the region of contact within } 6 \mu\text{m} \text{ near the cell front and rear} \\ 0 & \text{otherwise;} \end{cases}$$

- (3) Uniform catch/slip bonds: $\partial N(t, s) / \partial t = k^+ \eta_0 (1 - N) - k^- N \exp\left(-\frac{\alpha |\mathbf{F}| / N}{k_B T}\right)$. where k^+ is a constant binding rate, η_0 is the unsaturated substrate ligand concentration, k^- is the zero-force unbinding rate, and α is a microscopic length scale characterizing the unbinding transition.

Bond rupture: A bond can break at any spatial or temporal location when the adhesive force per bond exceed a critical threshold load, F_{critical} .

Bond formation: The pseudopod is prevented from interaction with the surface until it reaches a minimal critical length, $L_{\text{pseudopod}}$. Once the length condition is met, proximity to the surface determines if bonds form between the pseudopod and the substrate. In the first two models for bond density, a bond forms with $N = 1$, while in the third model, the initial bond density per site is $N = (k^+ \eta_0) \Delta t$ where Δt is the numerical time step.

Discretization of the model

To simulate the dynamics of a crawling cell, the membrane-cortex structure is spatially discretized using 162 points and every discrete point has its own position and velocity field. The temporal discretization is $\Delta t = 1.788 \times 10^{-4}$ seconds and the averaged spatial discretization is $\Delta s = 0.4 \mu\text{m}$. Every time instance, local forces are computed at every discretized point along the membrane-cortex structure and its position is updated according to the local force balance described in Eq. S1. A first order finite difference scheme is used to evaluate spatial derivatives. Forward Euler method is used to evolve the force balance equation at each point on the structure. The cell achieves an equilibrated shape before migration is initiated. Model parameters are provided in supplementary material, Table S1.

S.3 Model parameters

We perform simulations using the baseline parameter values listed in Table S1. Where possible, parameter values are chosen to be roughly the same order of magnitude as measured or estimated values in literature. However, some model parameters are not experimentally measurable, and below we give a brief discussion of our estimates of these parameters.

The radius for a spherical *Dictyostelium* in the absence of adhesions to the surface is set in the simulation, $R_0 = 7.56 \mu\text{m}$, in order to yield a crawling cell length of around $20 \mu\text{m}$. *Dictyostelium discoideum* amoebas are known to be pressurized due to the contraction of the actomyosin network of the cortex. In our model, the resting tension (γ) in the membrane-cortex structure is mostly composed of the cortical tension. Our value of the resting tension in Table S1. is in good agreement with previous measurements of the cortical tension that reported an approximate value of $1000 \text{ pN}/\mu\text{m}$ [5, 11–13]. The measurements were obtained from micropipette aspiration experiments and approximations from Laplace’s law with given hydrostatic pressure differential. Without more reliable measurements of the elastic properties of *Dictyostelium* membrane and cortex, we chose the elastic parameter k to be the same as the resting tension so that deformation forces are comparable to forces from tension. For a given set of forces, the drag coefficient determines the resulting crawling velocity and thus, is set to match the timescale of biological motion, $\xi = 72 \text{ pN s}/\mu\text{m}^3$.

Little is known about the binding receptors in *Dictyostelium*. Although the *Dictyostelium* genome does not carry any genes for integrins, we compare the parameters of the catch bond dynamics model to experimental values for other cell types with integrin-mediated adhesions. In [15], the catch bond between the extracellular matrix component fibronectin (FNIII_{7–10}) and the cellular integrin ($\alpha_5\beta_1$) is found to have a zero-force unbinding rate of $k^- = 55 \text{ s}^{-1}$, while the binding rate ranges between $k^+\eta_0 = 1 - 10 \text{ s}^{-1}$.

The coefficients of polymerization force driving pseudopod extension are unspecified for *Dictyostelium*. The values of listed in Table S1 were chosen to overcome the strength of adhesion forces and reproduce migration speeds of approximately the scale observed in the experiments. The minimal length of the pseudopod for attachment was chosen to be consistent with [2, 3, 5, 14] (reported between $6\text{--}12 \mu\text{m}$).

S.4 Perturbations to mechanical parameters

We performed a series of simulations of cells with perturbations to mechanical parameters by varying the elastic spring constant, k , and resting tension, γ , of the membrane-cortex structure but also the first constant of the polymerization force, ρ_1 . The resulting averaged cell speed, period of motility cycle, and cell length are reported below in Table S2. The stride length is computed from the average cell speed and period of motility cycle, $\lambda = V/f$.

Symbol	Definition	Numerical value
γ	Resting tension for membrane-cortex link	800 pN/ μm
k	Elastic stiffness for membrane-cortex link	800 pN/ μm
κ_{cell}	Bulk modulus	800 kPa
k_{steric}	Constant for cell-substrate steric interaction	80 kPa
δ_w	Steric separation distance	0.6 μm
ζ	Adhesion site strength	800 pN/ μm^2
ℓ_0	Resting spring length	0.4 μm
$k^+ \eta_0$	Binding rate	16.1074 s $^{-1}$
k^-	Zero-force unbinding rate	322.1460 s $^{-1}$
α	Length scale of unbinding transition	$1.25 \times 10^{-4} \mu\text{m}^2/\text{pN}$
F_{critical}	Threshold adhesive force	8400 pN/ μm^2
$L_{\text{pseudopod}}$	Pseudopod minimal length for attachment	10 μm
ρ_1	Polymerization constant	11.5556 $\mu\text{m}/\text{s}$
ρ_2	Polymerization constant	0.0082 $\mu\text{m}^2/\text{pN}$
ρ_3	Polymerization constant	1.1111 $\mu\text{m}/\text{s}$

Table S1: Definition and values of parameters for crawling simulation.

S.5 Parameters relevant for stride length in the model

Fig. 7 suggests that cells perturbed from baseline parameters not only use stepping motility but do so by approximately preserving their stride length, $\lambda = 12 \mu\text{m}$. We note that perturbations considered in Fig. 7: the resting tension, the elastic spring constant, and the strength of polymerization (ρ_1), do not alter the stride length of the motility cycle. For this exploration, we identify which parameters in our model that could determine this emergent length scale, λ . In particular, we show that the criteria used for pseudopod length for attachment ($L_{\text{pseudopod}}$) and the threshold rupture load in the adhesive force (F_{critical}) are two parameters that can change the stride length in our model (see Fig. S2).

For individual variations of the two parameters, threshold rupture load and pseudopod attachment length, we performed a series of simulations with perturbations to cellular parameters. The mean speed of migration and the frequency of the motility cycle are evaluated for each set of simulations and a stride length is computed through a linear fit, $v = \lambda \cdot f$ (as shown in Fig. S2 B, C). We find that decreasing the threshold rupture load from its baseline value (F^*) or the pseudopod length from its baseline value (L^*) results in smaller stride length (Fig. S2A). For this parameter regime, increasing the threshold rupture load results in no locomotion while increasing the pseudopod length results in a larger stride length. The baseline values for these two parameters are provided in Table S1 (specifically, $F^* = 8400 \text{ pN}/\mu\text{m}^2$ and $L^* = 10 \mu\text{m}$). Thus, there is a positive relation between the stride length and threshold rupture load per bond but also between the stride length and the pseudopod attachment length.

S.6 A gradual slip response

Instead of a sharp threshold rupture load, F_{critical} , for the slip response of the bond dynamics in Eq. 5, one could model the slip response with a gradual force-sensitivity as described in [15]:

$$\frac{\partial}{\partial t} N(t, s) = k^+ \eta_0 (1 - N) - k_c^- N \exp\left(-\frac{\alpha |\mathbf{F}|/N}{k_B T}\right) - k_s^- N \exp\left(\frac{\beta |\mathbf{F}|/N}{k_B T}\right). \quad (\text{S11})$$

Description	Numerical value	Speed ($\mu\text{m}/\text{min}$)	Period (min)	Cell length (μm)	Stride length ($\lambda = V/f$)
Baseline cell		11	1.1	31	12
Tension ⁺⁺ mutant	$\gamma = 960 \text{ pN}/\mu\text{m}$	16	0.7	25	11
Tension ⁺ mutant	$\gamma = 880 \text{ pN}/\mu\text{m}$	13	0.9	28	12
Tension ⁻ mutant	$\gamma = 720 \text{ pN}/\mu\text{m}$	8	1.7	35	13
Tension ⁻⁻ mutant	$\gamma = 640 \text{ pN}/\mu\text{m}$	<2	–	39	–
Elastic stiffness ⁺⁺ mutant	$k = 960 \text{ pN}/\mu\text{m}$	9	1.3	33	12
Elastic stiffness ⁺ mutant	$k = 880 \text{ pN}/\mu\text{m}$	9	1.3	32	12
Elastic stiffness ⁻ mutant	$k = 720 \text{ pN}/\mu\text{m}$	12	0.9	29	11
Elastic stiffness ⁻⁻ mutant	$k = 640 \text{ pN}/\mu\text{m}$	16	0.70	26	11
Polymerization ⁺⁺ mutant	$\rho_1 = 1664 \text{ pN}/\mu\text{m}^2$	17	0.7	32	12
Polymerization ⁺ mutant	$\rho_1 = 1248 \text{ pN}/\mu\text{m}^2$	15	0.8	32	12
Polymerization ⁻ mutant	$\rho_1 = 624 \text{ pN}/\mu\text{m}^2$	5	–	32	–
Polymerization ⁻⁻ mutant	$\rho_1 = 416 \text{ pN}/\mu\text{m}^2$	<2	–	29	–

Table S2: Motility changes due to variations in cell mechanical parameters

Here, $k_c^- = k^-$ is the zero-force unbinding rate for the catch response, while k_s^- is the zero-force unbinding rate for the slip response, and β is a microscopic length scale characterizing the unbinding transition for the slip response. We fix the unbinding rate for the slip response, k_s^- , to be an order magnitude smaller than the unbinding rate for the catch response. This ensures that in the low applied force regime, the catch response is the dominant behavior as it was in the previous slip model. The emergent behavior for different values for the unbinding transition length scale are presented in Fig. S3. Below, we assess the effect of this gradual slip response model on the emergent motility illustrated in Fig. 6.

Simulations with bond dynamics given by Eq. S11 show that depending on the β parameter, all three modes can also be captured by this model: stuck (Fig. S4 B), stepping (Fig. S4 C, D), and gliding (Fig. S4 E). The emergent stepping motility mode is reported by the spatiotemporal patterns of the axial traction stresses and the time evolution of the cell length (Fig. S4 F, G) which quantitatively agree with those obtained with a sharp slip response in Fig. 6 A, B.

We note that the transition between motility modes with varying the unbinding transition length scale, β , is phenomenologically the same as the transition with threshold rupture load seen through vertical changes in Fig. 8. With a sharp slip response, our model predicted that decreasing the threshold rupture load results in weakened adhesions and a transition to a gliding-like locomotion. A large value for β results in adhesions which rupture with lower applied forces. For these larger values for β is also the regime where gliding-like locomotion is reported in the improved bond dynamics model (see Fig. S3). This result suggests that the catch response and not the slip response of the adhesive bonds is instrumental to capture the observed cyclic oscillations in cell length and the spatiotemporal patterns of the axial traction forces.

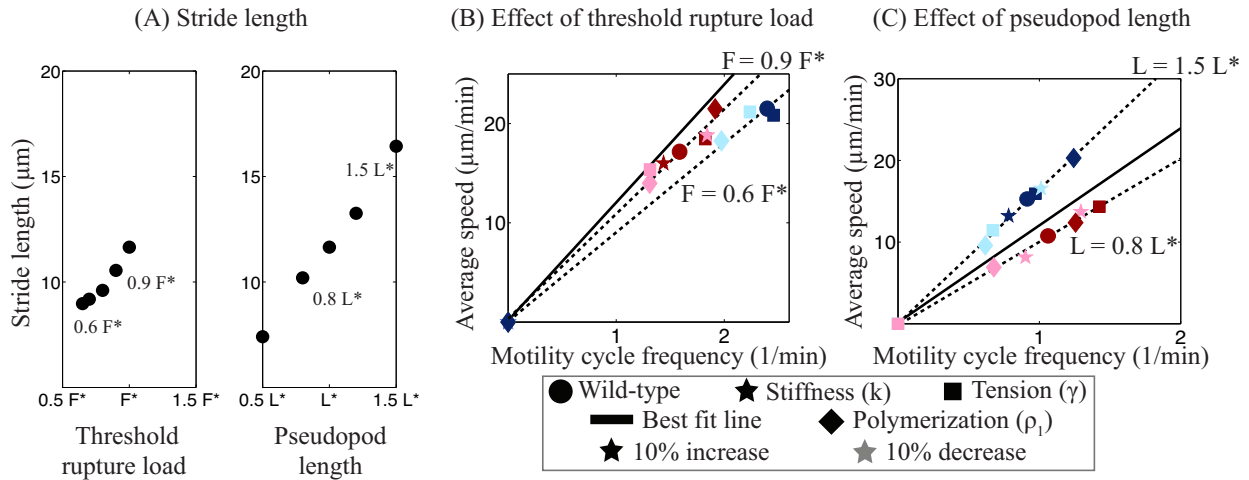


Figure S2: **The threshold rupture load and the length for pseudopod attachment are two parameters that determine the emergent stride length.** (A) The stride length is plotted as a function of both the threshold rupture load per bond and the pseudopod length required for attachment. The stride length is observed to be proportional to either of the two parameters varied. L^* and F^* denote the baseline values for the two parameters, pseudopod length and critical rupture load, respectively, which are reported in Table S1. (B,C) For two variations of the critical rupture load (B) and two variations of the pseudopod length (C), the mean speed of migration as a function of the frequency of the motility cycle are plotted for cells with perturbations to cellular parameters. The dashed lines are the least squares fit to the data points, while the solid line is the least squares fit for the baseline data replotted from Fig. 7. Darker colors indicate increases from baseline cellular parameters while lighter colors indicate decreases from the baseline parameters.

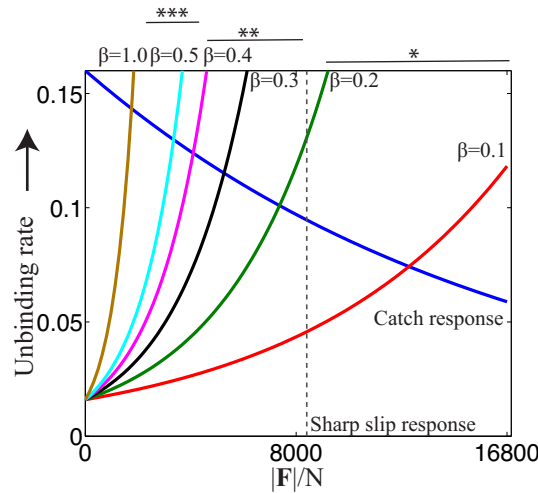


Figure S3: **The unbinding rate of a bond is plotted as a function of the applied force density.** The blue curve denotes the unbinding rate due to the catch response, while the dotted gray line shows the sharp unbinding rate due to the slip response in our model. Instead of a sharp slip response, one could model the slip unbinding rate with varying gradual response curves: $\beta = 0.1, 0.2, 0.3, 0.4, 0.5, 1$. For low values of the β parameter, the cell is stuck to the surface and cannot overcome adhesive forces (*), and as the β parameter is increased, stepping motility emerges (**). For even larger values of β , the cell is seen to undergo small amplitude length oscillations indicative of gliding motility mode (***) .

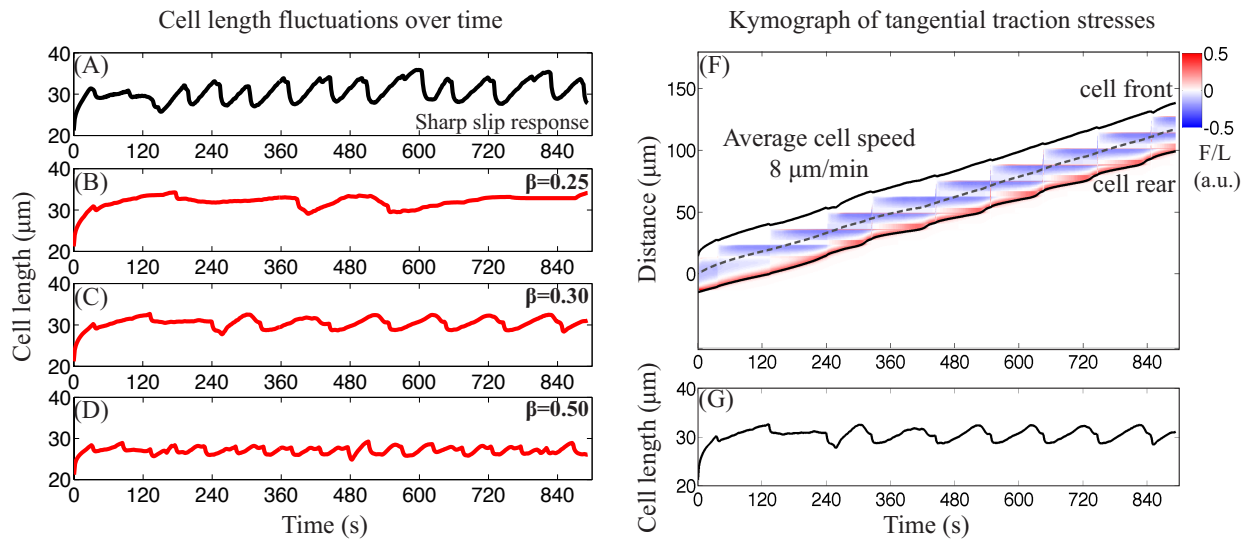


Figure S4: **All three amoeboid motility modes emerge in a model of bond dynamics with a gradual slip response.** For various slip response in bond dynamics, the cell length over time is reported in panels (A)-(D). The cyclic length oscillations reported in the paper with a sharp slip response are reproduced for comparison in (A), while panels (B)-(D) illustrate the type of behavior that can emerge from a gradual slip response with varying values for the β parameter: (B) $\beta = 0.25$ (stuck), (C) $\beta = 0.30$ (stepping), (D) $\beta = 0.5$ (gliding). (F) Kymograph of the tangential traction stresses as a function of the position along the cell trajectory at a given time for a cell with bond dynamics modeled by Eq. S11 and $\beta = 0.30$. The inclined lines indicate the instantaneous position of the front and rear cell edges while the dashed line represents the cell centroid position. (G) The time evolution of the cell length shows periodic extension-contraction events for a cell with bond dynamics modeled by Eq. S11 and $\beta = 0.30$.

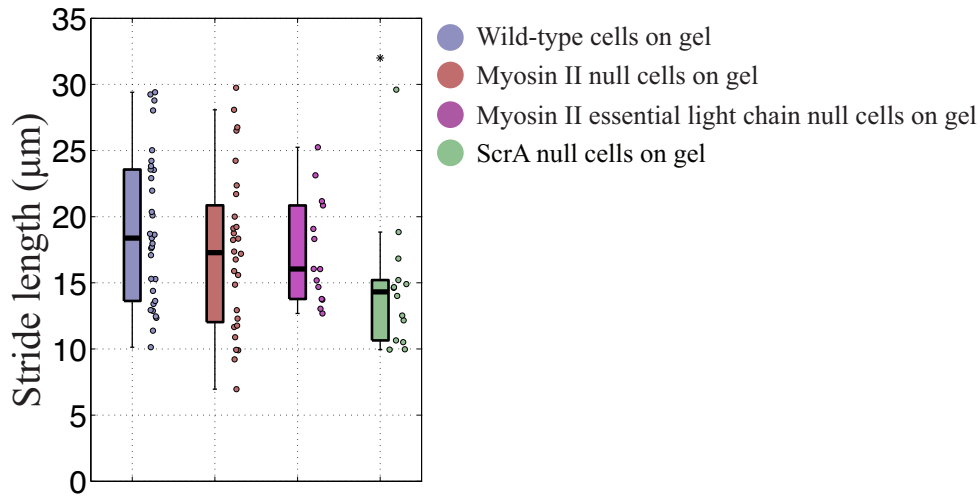
Supplementary Figures:

Figure S5: **Box and whisker plot of the stride length for different cell types.** The boxplots show the quartiles and the median of the distribution of stride length, defined as $\lambda = vf$ where v is the average cell speed and f is the frequency of the motility cycle. The circles represent the value of the stride length for each individual cell in each group. One asterisk denotes statistically significant differences between the medians of two distributions ($p < 0.05$, Wilcoxon ranksum test).

Supplementary Movies:

Supplementary movie 1: **Simulated cell exhibits gliding-like motility when cell-surface interaction is modeled by linearly elastic springs.** Top panel shows the instantaneous cell outline along with the axial traction stresses. The inset is a zoom in view of the ventral part of the cell to show the spatiotemporal dynamics of adhesions. Cell length is plotted as a function of time in the bottom panel.

Supplementary movie 2: **Stepping locomotion is exhibited by a cell with mechanosensitive adhesions to the surface.** Top panel shows the instantaneous cell outline along with the axial traction stresses. The inset is a zoom in view of the ventral part of the cell to show the spatiotemporal dynamics of adhesions. The color and width of the adhesion links is linearly scaled to the bond density; a dark, black link corresponds to full occupancy, i.e., $N = 1$, and lighter, thinner links indicate low density bonds. Cell length is plotted as a function of time in the bottom panel.

Supplementary movie 3: **Transitions in emergent motility modes are reported as a function of the surface binding site density.** For different surface binding site densities, the left-hand side plots show the time evolution of cell length while the right-hand side plots show the instantaneous cell outline along with the axial traction stresses. Four different values of surface binding site density are considered in order of increasing value: $\eta_0 = 0.006, 0.012, 0.016, 0.024$. At low binding site density (top panel), the average cell speed is $20 \mu\text{m}/\text{min}$ and the motion shows small amplitude oscillations in length changes. The identification of the motility mode as gliding is based on the small amplitude of morphological changes (less than $2 \mu\text{m}$). As binding site density is increased, we observe a switch in migration mode from gliding to transition (second panel) to stepping (third panel). The identification of the motility mode as gliding is based on the amplitude of morphological changes (average amplitude between $5\text{-}8 \mu\text{m}$). The mean cell speed decreases while the amplitude of length oscillations

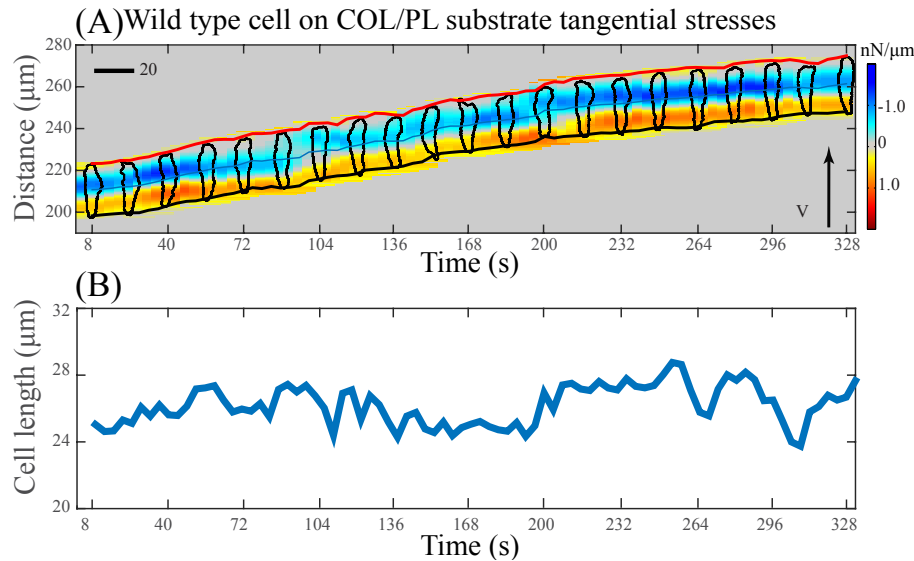


Figure S6: **Gliding-like motility mode in wild-type *Dictyostelium* cells migrating on highly adhesive substrate.** The identification of the motility mode is based on the spatiotemporal patterns of axial traction stresses and small amplitude length changes. (A) Axial traction tension kymograph of a representative chemotaxing wild-type *Dictyostelium* cell on a highly adhesive substrate additionally coated with poly-L-lysine (COL/PL). Cell contour is represented in black. The color map on the right indicates the magnitude of the tangential stresses. The red and black lines indicate the instantaneous front and back edges of the cell respectively while the gray line indicates the instantaneous position of the cell centroid. (B) The corresponding cell length plotted over time shows small amplitude length changes characteristic of a gliding motility mode.

increases. If binding site density is further increased, the cell does not migrate across the surface and its length reaches a plateau value. The motility mode is classified as stationary since the average speed is below $2 \mu\text{m}/\text{min}$.

Supplementary movie 4: **Simulated cells exhibits recycling of adhesion sites when cell-surface interaction is modeled by non-uniform linearly elastic springs.** The movie shows the instantaneous cell outline along with the axial traction stresses for a cell adhering to the surface only near the cell front and rear. At the end of the motility cycle, what was initially the front adhesion site is now located at the rear of the cell and the cell pulls upward and inward on these adhesion bonds.

Supplementary References

- [1] Alonso-Latorre, B., J. C. del Álamo, E. Bastounis, R. Meili, R. A. Firtel, and J. C. Lasheras, 2010. Spatiotemporal analysis of traction work produced by migrating amoeboid cells. *Biophys J.* 98:367a-367a.
- [2] Bastounis, E., R. Meili, B. Alonso-Latorre, J. Francois, J. C. del Álamo, J. C. Lasheras, and R. A. Firtel, 2011. The SCAR/WAVE complex is necessary for proper regulation of traction stresses during amoeboid motility, *Mol. Biol. Cell.* 22:3995-4003.
- [3] Bastounis, E., R. Meili, B. Álvarez-González, J. Francois, J. C. del Álamo, R. A. Firtel, and J. C. Lasheras, 2014. Both contractile axial and lateral traction force dynamics drive, *J. Cell Biol.* 204:1045-1061.
- [4] del Álamo, J. C., R. Meili, B. Alonso-Latorre, J. Rodríguez-Rodríguez, A. Aliseda, R. A. Firtel, and J. C. Lasheras, 2007. Spatio-temporal analysis of eukaryotic cell motility by improved force cytometry. *Proc. Nat. Acad. Sci. USA.* 104:13343-13348.

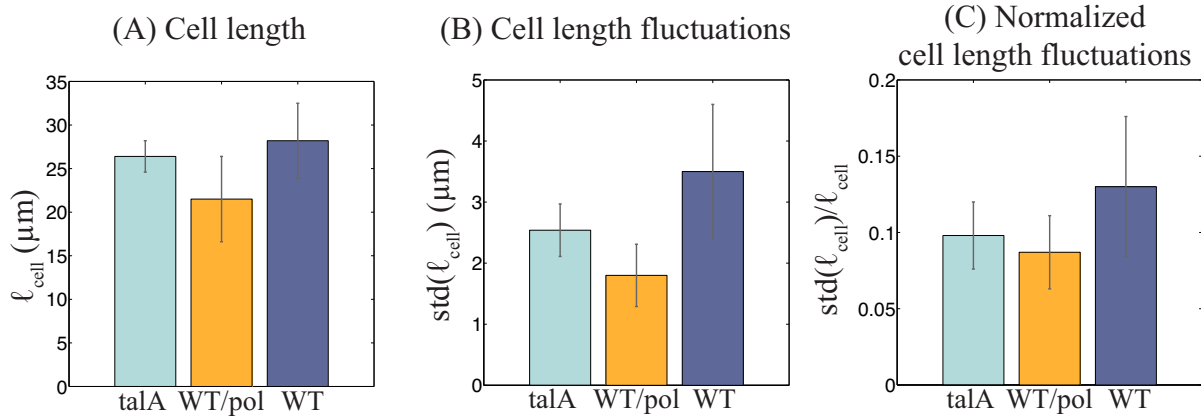


Figure S7: Talin A-null cells show small length changes similar to those observed in cells on poly-L-lysine coated surfaces. The cell lines considered are wild-type (WT) and talin A-null (talA) cells on collagen gel, and wild-type cells on poly-L-lysine coated surfaces (WT/pol) ($N = 6$ for all three cell types). (A) Bar plot of cell length. Wild-type cells on collagen are significantly longer than wild-type cells on poly-L-lysine ($p = 0.012$) but not than talin A-null cells on collagen ($p = 0.36$). (B) Bar plot of standard deviations of cell length temporal fluctuations. Wild-type cells on collagen have significantly larger fluctuations than wild-type cells on poly-L-lysine ($p = 0.002$). There is a trend for wild-type cells on collagen to have larger fluctuations than talin mutants on collagen but it is not statistically significant ($p = 0.076$). (C) Bar plot of standard deviations of cell length normalized with cell length. Wild-type cells on collagen have significantly larger normalized fluctuations than wild-type cells on poly-L-lysine surfaces ($p = 0.041$). There is a trend for wild-type cells on collagen to have larger normalized fluctuations than talin mutants on collagen but it is not statistically significant ($p = 0.16$). Small normalized length fluctuations are observed in both talin A-null mutants and cells on poly-L-lysine, which exhibit a gliding motility mode.

- [5] Álvarez-González, B., R. Meili, E. Bastounis, R. A. Firtel, J. C. Lasheras, and J. C. del Álamo, 2015. Three-dimensional balance of cortical tension and axial contractility enables fast amoeboid migration, *Biophys. J.* 108:1-12.
- [6] Alonso-Latorre, B., R. Meili, E. Bastounis, J. C. del Álamo, R. A. Firtel, and J. C. Lasheras, 2009. Distribution of traction forces and intracellular markers associated with shape changes during amoeboid cell migration. 31th Annual International Conference of the IEEE Engineering in Medicine and Biology Society. 3346-3349.
- [7] Tse, J. R. and A. J. Engler, 2010. Preparation of hydrogel substrates with tunable mechanical properties. *Current protocols in cell biology / editorial board*, J. S. Bonifacino et al. Chapter 10:Unit 10-16.
- [8] Wang, Y. L. and R. J. Pelham, Jr., 1998. Preparation of a flexible, porous polyacrylamide substrate for mechanical studies of cultured cells. *Methods in enzymology*. 298:489-496.
- [9] Engler, A., L. Bacakova, C. Newman, A. Hategan, M. Griffin, and D. Discher, 2004. Substrate compliance versus ligand density in cell on gel responses. *Biophys. J.* 86:617-28.
- [10] del Álamo, J. C., R. Meili, B. Álvarez-González, B. Alonso-Latorre, E. Bastounis, R. A. Firtel, and J. C. Lasheras, 2013. Three-dimensional quantification of cellular traction forces and mechanosensing of thin substrata by Fourier traction force microscopy. *PLoS ONE*. 8:e69850.
- [11] Dai, J., H. P. Ting-Beall, R. M. Hochmuth, M. P. Sheetz, and M. A. Titus, 1999. Myosin I contributes to the generation of resting cortical tension. *Biophys. J.* 77:1168-1176.
- [12] Gerald, N., J. Dai, H. P. Ting-Beall, and A. De Lozanne, 1998. A role for *Dictyostelium* racE in cortical

- tension and cleavage furrow progression. *J. Cell Biol.* 141:483-492.
- [13] Reichl, E. M., Y. Ren, M. K. Mophew, M. Delannoy, J. C. Effler, K. D. Girard, S. Divi, P. A. Iglesias, S. C. Kuo, and D. N. Robinson, 2008. Interactions between myosin and actin crosslinkers control cytokinesis contractility dynamics and mechanics. *Curr. Biol.* 18:471-480.
- [14] Van Haastert, P. J. M, 2010. Chemotaxis: insights from the extending pseudopod. *J. Cell Sci.* 123:3031-3037.
- [15] Novikova E. A., and C. Storm, 2013. Contractile fibers and catch-bond clusters: a biological force sensor? *Biophys. J.* 105:1336-1345.
- [16] Mogilner A., and G. Oster, 1996. Cell motility driven by actin polymerization. *Biophys J.* 71:3030-3045.
- [17] Parekh S. H., O. Chaudhuri, J. A. Theriot, D. A. Fletcher, 2005. Loading history determines the velocity of actin-network growth. *Nat. Cell Biol.* 7:1219-1223.
- [18] Prass M., K. Jacobson, A. Mogilner, M. Radmacher, 2006. Direct measurement of the lamellipodial protrusive force in a migrating cell. *J. Cell Biol.* 174:767-772.
- [19] Heinemann F., H. Doschke, M. Radmacher, 2011. Keratocyte lamellipodial protrusion is characterized by a concave force-velocity relation. *Biophys. J.* 100:1420-1427.